.

A new electron-ion coincidence 3D momentum-imaging method and its application in probing strong field dynamics of 2-phenylethyl-N, N-dimethylamine

Lin Fan, Suk Kyoung Lee, Yi-Jung Tu, Benoît Mignolet, David Couch, Kevin Dorney, Quynh Nguyen, Laura Wooldridge, Margaret Murnane, Françoise Remacle, H. Bernhard Schlegel, and Wen Li

A new electron-ion coincidence 3D momentum-imaging method and its application in probing strong field dynamics of 2-phenylethyl-*N*, *N*-dimethylamine

Lin Fan,[1] Suk Kyoung Lee,[1] Yi-Jung Tu,[1] Benoît Mignolet,[2] David Couch,[3] Kevin Dorney,[3] Quynh Nguyen,[3] Laura Wooldridge,[3] Margaret Murnane,[3] Françoise Remacle,[2] H. Bernhard Schlegel,[1] and Wen Li[1,a)]

[1]*Department of Chemistry, Wayne State University, Detroit, Michigan 48202, USA*
[2]*Department of Chemistry, B6c, University of Liege, B4000 Liege, Belgium*
[3]*JILA and University of Colorado at Boulder, Boulder, Colorado 80303, USA*

We report the development of a new three-dimensional (3D) momentum-imaging setup based on conventional velocity map imaging to achieve the coincidence measurement of photoelectrons and photo-ions. This setup uses only one imaging detector (microchannel plates (MCP)/phosphor screen) but the voltages on electrodes are pulsed to push both electrons and ions toward the same detector. The ion-electron coincidence is achieved using two cameras to capture images of ions and electrons separately. The time-of-flight of ions and electrons are read out from MCP using a digitizer. We demonstrate this new system by studying the dissociative single and double ionization of PENNA (2-phenylethyl-*N*,*N*-dimethylamine). We further show that the camera-based 3D imaging system can operate at 10 kHz repetition rate. *Published by AIP Publishing.* [http://dx.doi.org/10.1063/1.4981526]

INTRODUCTION

The coincidence detection of photoelectrons and photoions arising from a single atom/molecule in gas phase is a powerful tool for untangling multi-channel ionization/dissociation dynamics. The early implementation of coincidence technique only provided energy information of each particle using time-of-flight methods.[1–4] Various position- and time-sensitive detectors were introduced to measure both the position and the time-of-flight (TOF) and thus enabled three-dimensional (3D) momentum detection of all particles.[5–12] Successful coincidence detection requires the count rate of the experiment to be less than one event per driving pulse (electron/ion/photon) to suppress false coincidence events. Velocity mapped imaging[13–15] was not initially developed to achieve the coincidence detection because it did not provide high resolution TOF information of individual particles. Instead, it used an imaging detector and a camera to measure the positions of particles with a relative large TOF range (nanosecond to 1 μs), which identifies the mass of the particles. Nonetheless, velocity map imaging (VMI) has become a very popular method in reaction dynamics, ultrafast spectroscopy, and other fields because of its relatively easy implementation and simultaneous measurement of energy and angular distribution of charge particles. Recently, a new type of VMI imaging system was developed to achieve 3D momentum detection with a conventional imaging detector.[16,17] In this system, a standard video camera was replaced with a fast frame complementary metal-oxide semiconductor (CMOS) camera (>1 kFrames/s) and the camera exposure is synchronized with the laser pulses

(>1 kHz) together with a waveform digitizer, which reads out the microchannel plates (MCP) pulse signal. In these coincidence experiments, because the count rate is low, a true coincidence between hit positions from the camera and TOFs extracted from the digitizer can be established to yield three coordinates (X, Y, t) required for 3D momentum (P_x, P_y, P_z) imaging. The demonstrated time resolution for this system is excellent (~30 ps). With this system, sliced velocity mapping of photoelectrons was achieved for the first time with an imaging detector. It was also demonstrated that the photoelectron-photoion coincidence could be achieved by accelerating electrons and ions simultaneously in a double-sided VMI setup towards two imaging detectors at the opposite ends of the spectrometer and applying the same 3D measurement scheme.[18] However, a conventional VMI apparatus features only one imaging detector and a uni-directional spectrometer. Is it possible to convert such apparatus to a photoelectron-photoion coincidence imaging apparatus? In this work, we will show that this is possible and the solution is quite simple with the camera-based 3D imaging system.

PENNA is a bifunctional molecule with a $-CH_2-CH_2-$ bridge linking the chromophore group (phenyl) and amine group. In the past decade, there has been great interest in studying the photoionization dynamics of PENNA. This is mainly because PENNA is one of the first molecules that was identified to support a new type of charge migration process that takes place at an extremely short time scale (a few hundreds of attoseconds to a few femtoseconds).[19–24] This charge transfer arises from a coherent superposition of a few electronic states of the cation and it occurs before any significant nuclear motion. Resonant two-photon ionization (R2PI) and Rydberg fingerprint spectroscopy have been used to study the slower intramolecular charge transfer (~80 fs)

a)wli@chem.wayne.edu

at different laser wavelengths.[19,22,25,26] However, such studies were limited to tens of femtosecond time resolution. A strong field IR-pump-IR-probe method has been proposed to observe the ultrafast charge migration with a resolution of few femtoseconds.[24] So far experimental investigations on the photoionization dynamics of PENNA under the intense laser field have been scarce. Furthermore, the dynamics of dissociation following ionization (single and double) are crucial for measuring molecular/recoil frame ionization rates because they show whether the axial recoil approximation is valid or not. With the axial recoil approximation, the recoil-frame ionization rate measurement is much simpler than those methods that require the pre-alignment of molecules. Here, we applied our new 3D electron-ion coincidence technique to study the strong field ionization/dissociation of PENNA with one laser. We have identified the dissociation pathways following the strong field double ionization of PENNA. This result will provide background information for future time-resolved studies.

EXPERIMENTAL SETUP AND COMPUTATIONAL METHODS

Experimental setup

An amplified Ti:sapphire femtosecond laser system was used to ionize the PENNA molecules in the mid-intensity strong field ($\sim 8 \times 10^{13}$ W/cm^2). The wavelength was 800 nm, and the repetition rate was 1500 Hz. The ultrashort laser pulse ($\sim$30 fs) was linearly polarized along the time-of-flight axis. For the one-camera setting, the experiment was carried out with a circularly polarized laser. PENNA (purity 98%) was purchased from Sigma-Aldrich and seeded in helium which is to be sent into the source chamber by a gas jet with 20 μm orifice. The PENNA sample was heated to $\sim$30 °C, and the gas jet was heated to $\sim$70 °C from outside of the source chamber. A skimmer with a 0.5 mm orifice was used to skim the center part of the expanded molecular beam before it entered the main chamber. The laser beam was sent into the main chamber perpendicularly with the molecular beam and the time-of-flight axis, and it was focused onto the molecular beam by a

concave mirror (f = 5 cm) inside the main chamber. A four-plate electron-ion optics was built to velocity map the electrons and ions arising from strong-field ionization. A short TOF length ($\sim$10 cm) was adopted to allow the detection of high-energy electrons. The timings of electrons and ions hitting the detector were picked off from the front MCP plate by a high-speed digitizer (National Instruments, PXIe 5162) through a signal-decoupling circuit. The maximum sampling rate of the digitizer is 5 GHz. The positions of electrons hitting the detector were recorded from the phosphor by a complementary metal-oxide semiconductor (CMOS) camera (Basler, acA640-750 μm). This camera (e$^-$) was set at $\sim$65 cm away from the detector, pointing at the center of the phosphor screen with a normal angle. Another CMOS camera (XIMEA, MQ013MG) was employed to record the ion positions. It was located at $\sim$120 cm away from the detector and slightly off-center of the screen. This camera's pointing direction had a $\sim$6° angle deviation to the screen normal. The justification for the use of two cameras is discussed in the section titled Results and Discussion. A schematic of the experimental setup is shown in Figure 1(a).

Computational methods

Electronic structure calculations were carried out with the development version of Gaussian[27] using the ωB97xD functional.[28] Relaxed potential energy scans were executed with the 6-31G(d) basis set.[29,30] The geometries of neutral PENNA, PENNA$^+$, PENNA^{2+}, transition states, and products were further optimized with the 6-311++G(d,p) basis set,[31] and their SCF energies were also calculated with this basis set. All optimized structures were checked by the normal mode vibrational analysis, and wave functions were tested for SCF stability. For PENNA dications, the identities of the open-shell singlet and triplet electronic configurations were confirmed by spin-squared expectation values ($\langle S^2 \rangle$) and spin density populations. GaussView[32] was used to visualize isodensity plots of the spin populations (isovalue = 0.004 a.u.). To explore the potential energy surfaces for dissociation of PENNA^{2+}, relaxed potential energy surface scans were performed by stretching the C–C bond and optimizing the remaining
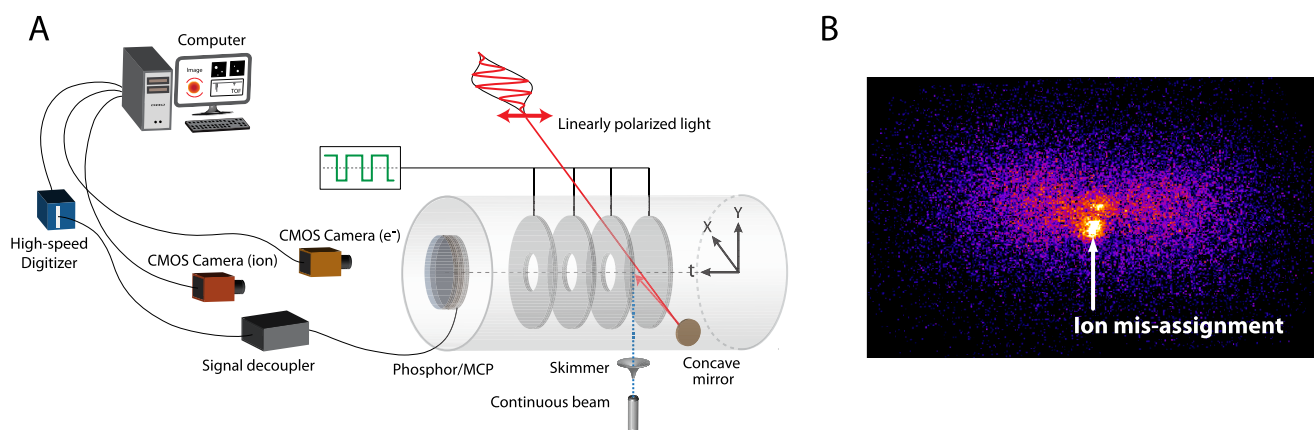

FIG. 1. (a) The schematic of the two-camera VMI setup that is capable of coincidence 3D momentum-imaging. The electrodes are pulsed to push both electrons and ions toward the imaging detector. (b) With a one-camera setup, the separation between electrons and ions is not complete. The main features are photoelectrons from the strong field ionization of PENNA using circularly polarized light.

coordinates. The transition state structures on the open-shell singlet and triplet surfaces of the dication were confirmed to have only one imaginary frequency by the vibrational mode analysis. To explore the closed-shell singlet potential energy surface of the dication, we started with the ground state geometry of PENNA, vertically ionized to the closed-shell singlet state of PENNA^{2+} and tracked the dissociation using Damped Velocity Verlet (DVV) reaction path following.[33] Up to the transition state, the closed shell singlet dication calculations had a closed-shell to open-shell instability and the wavefunction optimized to the lower energy open-shell singlet dication.

The photoelectron spectrum has been computed by modeling the photoexcitation and photoionization dynamics induced by a 22 fs 800 nm IR pulse with a field strength of 10^{12} W/cm^2 in the PENNA molecule at a frozen geometry. The time-dependent Schrödinger equation was numerically integrated using a basis of neutral and ionized electronic states.[24,34] The electronic structures of the lowest 30 neutral states were computed at the TDDFT ωB97xD/6–311++G(d,p) level. A dense manifold of excited states is required to accurately describe the multiphoton excitation and ionization of the PENNA ground state. The ionized states are described as the anti-symmetrized product of the field-free cationic electronic states and the wavefunction of the ionized electron which is described by a plane wave. This approximation can affect the photoelectron spectrum, especially at low kinetic energy because the interaction between the ionized electron and the cationic core is neglected, and over-the-barrier and tunnel ionizations are not accounted for. The ten lowest cationic states are computed at the ωB97xD/6–311++G(d,p) level. The ionization continua are discretized both in energy (from 0 to 25 eV) and angular distribution. In total, there are 18 000 ionized states and 30 neutral states in the basis. To account for the random orientation of the molecules, we computed the dynamics for a set of 50 randomly oriented molecules. From the amplitudes of the ionized states, we computed the photoelectron spectrum averaged over the orientation.

RESULTS AND DISCUSSION

Achieving 3D coincidence measurement with a single imaging detector

To upgrade a conventional VMI to a coincidence 3D momentum imaging apparatus, we need to address two issues associated with it. The first issue is the uni-directional spectrometer of a conventional VMI apparatus. It can normally be run either in photoelectron or photoion mode by applying different voltages on the electrodes. To image both ions and electrons at the same detector, the voltages of electrodes should be switched very quickly to accelerate both particles toward the same direction. This has been demonstrated by Janssen and co-workers by pulsing the electrodes and employing a delay line detector.[35] Owing to the large mass difference between electrons and ions, the electron can maintain the same imaging condition as with non-pulsing electrodes while ions suffer minimum momentum blurring (SIMION simulation ~1%). Once ions and electrons arrive at the imaging detector, they both produce flashes on the phosphor screen, which are then

captured by the camera in the same frame. However, how to associate the positions and measured TOFs is not trivial. Previously, in either ion or electron mode, the brightness of the camera flash shows a strong correlation with the intensity of the TOF peak in the digitized waveform.[16] This was exploited to associate the positions and TOFs in a multi-hit event. In Figure 1(b), it is shown that because the correlation slopes are different for electrons and ions, this scheme can lead to some mis-assignment of ions in the electron image (or vice versa) when processing frames containing both electrons and ions.

The solution to this is to add one additional camera. Because the large difference between the TOFs of the electrons (<100 ns) and those of ions (>1 μs), one camera can be triggered to only expose for the first 200 ns after the laser pulse to capture electrons while the second camera starts to expose after 500 ns to only image ions. With this configuration (Figure 1(a)), the association between the time and position of the charged particles becomes quite easy and self-evident: the positions of particles in the electron camera are associated with the electron TOFs while those positions on the ion camera with the ion TOFs. Both TOFs are measured by digitizing the MCP output with a single high-speed digitizer. If there are multi-hit events such as in dissociative double ionization, the brightness-intensity correlation can now be applied to each camera frame separately, as shown previously either in electron or ion detection mode. With this new scheme, we can achieve the complete separation of electrons and ions and this enables the ion-electron coincidence 3D imaging measurement for the first time using a single imaging detector. We estimated the spatial and temporal resolutions to be 6% and 1% for ions and 3% and 3% for electrons, respectively. In Figures 2 and 4, we showed the results of the ion-electron double coincidence measurement of the PENNA single ionization and electron-ion-ion triple coincidence of PENNA dissociative double ionization.

Single ionization of PENNA

The previous ion mass spectrum of PENNA in an intense laser field showed that the dimethylamine monocation (N(CH$_3$)$_2$CH$_2^+$, mass 58) is the major product while the yield of the parent ion is much lower than N(CH$_3$)$_2$CH$_2^+$ (~0.05), which suggested that most parent cations are unstable.[36] Figure 2(a) shows the momentum distribution of N(CH$_3$)$_2$CH$_2^+$ in the plane perpendicular to the laser polarization while Figures 2(b) and 2(c) show the momentum distributions of electrons in coincidence with N(CH$_3$)$_2$CH$_2^+$ in the plane perpendicular and parallel to the laser polarization, respectively. The electron energy distribution is shown in Figure 3(a). It has been showed previously that the single ionization of PENNA could populate three different electronic states D$_0$, D$_1$, and D$_2$, with the differences in ionization energies being less than one photon energy (1.6 eV).[36] The dissociations of the excited states D$_1$ and D$_2$ are through a series of conical intersections to the D$_0$ state, and the main product is N(CH$_3$)$_2$CH$_2^+$. The kinetic energy release (KER) of the ion matched well with that of calculations.[36] In Figure 3(a), we show the electron energy distribution and its comparison with the photoelectron spectrum resulting from frozen geometry simulations of the electron dynamics of randomly oriented molecules, which
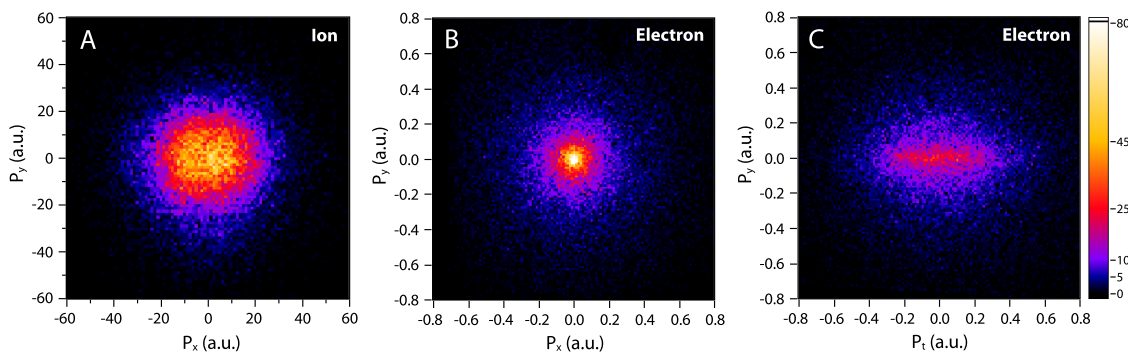
FIG. 2. (a) XY momentum distribution of the dimethylamine monocation ($N(CH_3)_2CH_2^+$). (b) XY momentum distribution of photoelectrons in coincidence with $N(CH_3)_2CH_2^+$. (c) Yt momentum distribution (t is the TOF axis) of the photoelectrons in coincidence with $N(CH_3)_2CH_2^+$.

takes into account the multiphoton excitation and ionization by the laser pulse, for more method details see Ref. 24. The agreement is good for high kinetic energy electrons (above 4 eV). The discrepancy at low kinetic photoelectron energy can be understood from the limitations of the model used in the simulations. The model only includes the multiphoton photoionization process and neglects the Coulomb interaction between the ionized electron and ionic core, which is known to produce low energy electrons by over-the-barrier or tunneling ionization. This result further suggests that in strong field ionization, the photoelectron spectrum alone is insufficient to identify the produced cation electronic states. A complete theoretical modeling of the strong field photoionization of big molecules such as PENNA is currently out of reach.

With the electron-ion coincidence measurement capability, we can produce the correlation map between the KER of the dissociated fragments and the electron kinetic energy (eKE) and this is shown in Figure 3(b). Interestingly, an apparent correlation can be seen (the diagonal structure). However, because the energy scale is different between the KER and eKE, it is unlikely that an energy conservation mechanism (as in single photon ionization) is at play. Upon further investigation, such a structure persists even for non-dissociative channels such as water single ionization, which suggests that the observed feature is not true correlation. However, we did observe a significant difference in momentum distributions of electrons in coincidence with monocations and dissociative dications (see Figures 2(c) and 4(c)). This validates our method for detecting coincidence events.

Double ionization and dissociation dynamics of PENNA

PENNA dications were not observed in the mass spectrum, and this suggests that all dications dissociate after production by the strong laser field. Triple coincidence (ion-ion-electron) was used to identify the dissociation products. We could employ the quadrupole coincidence (ion-ion-electron-electron) because the current method is capable of highly efficient detection of two electrons.[37] However, two-electron measurements do not provide further insight into the scope of this study while they require a much longer acquisition time. Therefore, we will focus on the triple coincidence data (Figure 4).

It can be readily identified from the photoion-photoion coincidence (PIPICO) map (Figure 5(a)) that the major dissociation channel leads to the dimethylamine monocation ($N(CH_3)_2CH_2^+$, mass 58) and benzyl monocation ($C_6H_5-CH_2^+$, mass 91). After applying momentum conservation criteria to remove false coincidence, we can cleanly select the ion pairs that arise from the dissociation of the PENNA dication. Figures 4(a) and 4(b) show momentum distributions of ions mass 58 and mass 91 after applying momentum conservation criteria in the plane perpendicular to the laser polarization while Figure 4(c) is the momentum distribution of coincidence electrons in the plane parallel to the laser polarization. The angular distributions of both ions are isotropic (spherical), which suggests that the dissociation time is longer than the rotation period. The total KER of the ion pairs is peaked around 2.9 eV and has a cutoff extending beyond 4 eV (Figure 5(b)).
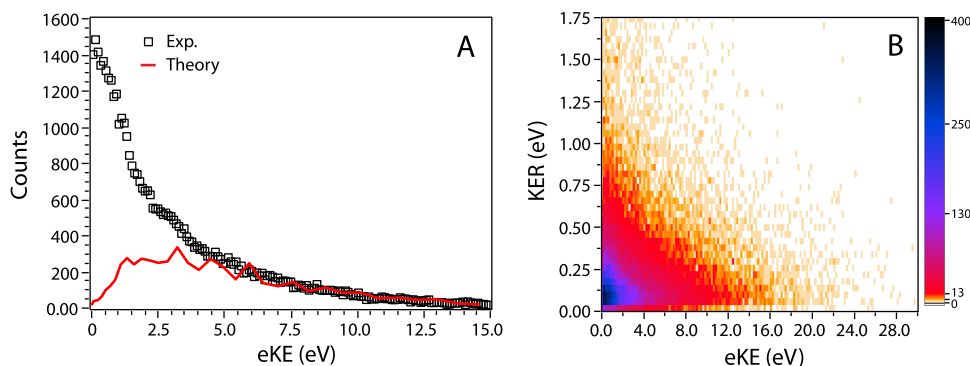

FIG. 3. (a) The photoelectron spectrum of single ionization (black) and comparison with theoretical simulations (red). (b) The energy correlation map between the ion KER and electron eKE.
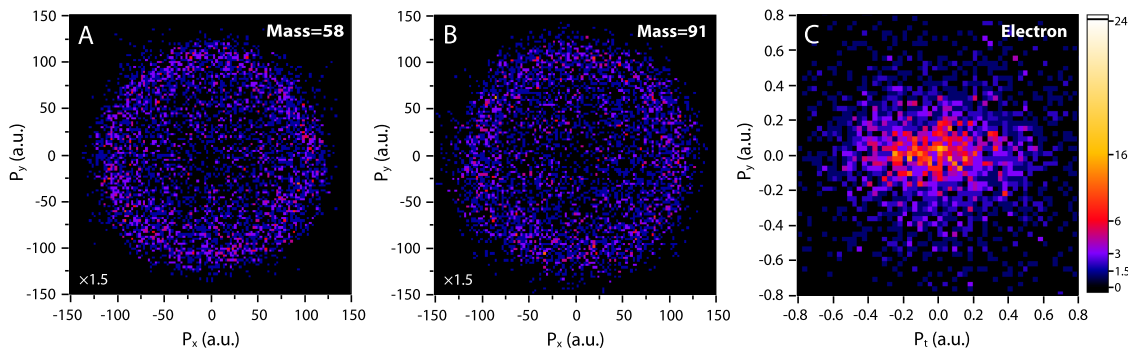
FIG. 4. XY momentum distributions of coincidence ion pairs of the (a) dimethylamine monocation ($N(CH_3)_2CH_2^+$, mass 58) and (b) benzyl monocation ($C_6H_5-CH_2^+$, mass 91). (c) Yt momentum distribution of photoelectrons in coincidence with the ion pairs.

Now we turn to the theory to help identify the dication states that are involved in the dissociation processes. The PENNA dication has three possible electronic structures: closed-shell singlet, open-shell singlet, and open-shell triplet. Density functional calculations were carried out to examine the electronic structures of PENNA^{2+}, transition states, and reaction paths for dissociation. We started with the ground state of neutral PENNA that was confirmed in previous studies.[19,24] From the neutral PENNA molecule, we calculated the adiabatically optimized geometries of the PENNA monocation and dications. Then, relaxed scans along the C–C bond stretching coordinate of PENNA dications were employed to explore the dissociation potential energy surfaces.

Closed-shell singlet PENNA dications are produced with two electrons removed from the same orbital, leading to an excited state while open-shell singlet dications have two electrons removed from different orbitals, resulting in diradicals. The relaxed scans for stretching the C–C bond of PENNA^{2+} show that closed-shell singlet PENNA dications merge with the singlet open-shell after it goes through the energy barrier, leading to the same products (Figure 6, inset). The energy of the triplet potential surface is higher than the singlet potential surface (Figure 6). The singlet transition state has a shorter C–C bond (1.92 Å) than the triplet transition state (2.17 Å), and the energy is 0.65 eV lower.
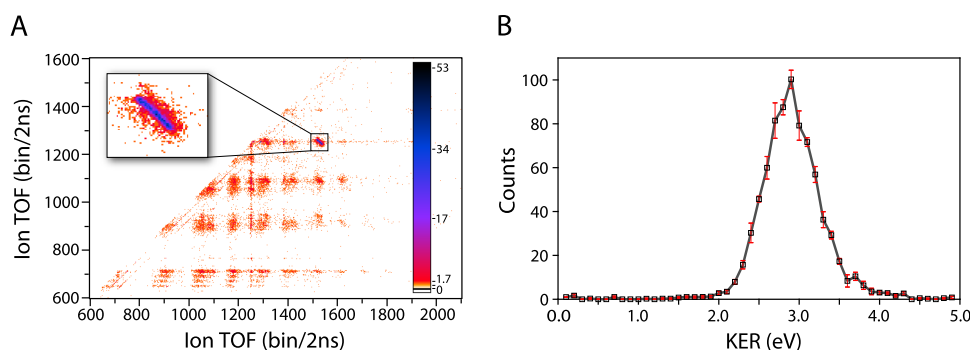

FIG. 5. (a) Photoion-photoion coincidence (PIPICO) map of the dissociative double ionization of PENNA. (b) The kinetic energy release distribution of mass 58 and 91 ion pairs from double ionization.
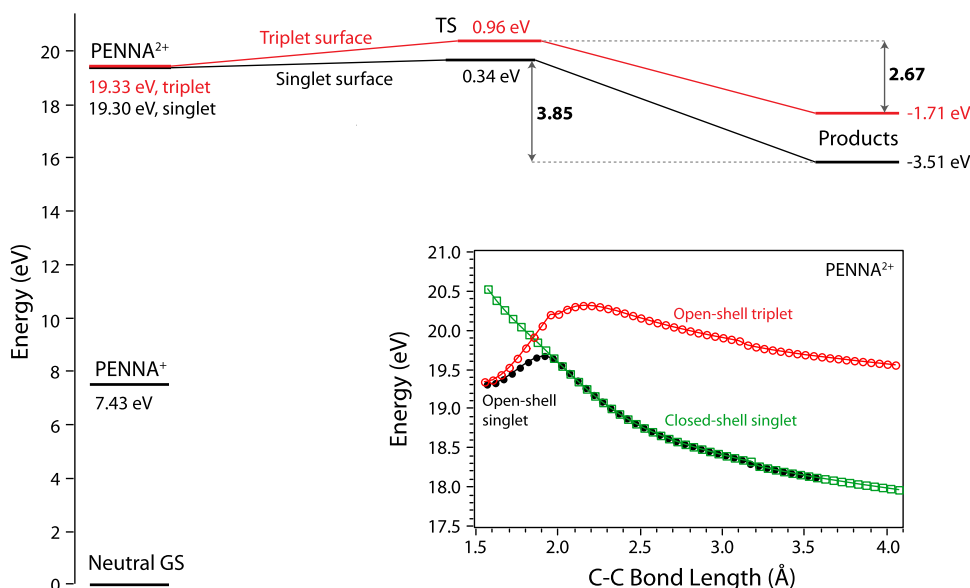

FIG. 6. Energy levels of PENNA dication open-shell states, transition states, and final products. The inset shows the relaxed potential energy surfaces along the C–C bond for different dication states.
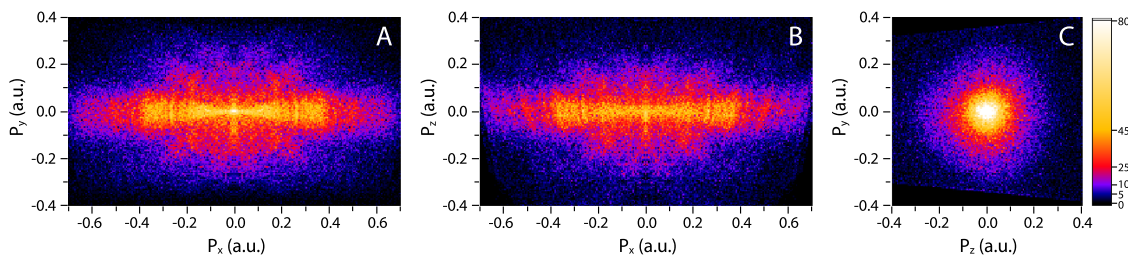
FIG. 7. 3D momentum distributions of photoelectrons arising from the strong field ionization of krypton by linearly polarized laser beams running at a 10 kHz repetition rate. The camera-based imaging system runs at 2 kFrames/s.

From the energy diagram, we can see that the reverse barrier for the open-shell singlet state is 3.85 eV, which is close to the measured maximum kinetic energy release (KER). The open-shell triplet state has a reverse barrier of only 2.67 eV, which is even smaller than the peak value of the measured KER. The open-shell singlet state also has a lower activation barrier (0.34 eV) than that of the open-shell triplet state (0.96 eV). Both facts prompt us to conclude that dissociation through the open-shell singlet is the dominant dissociation channel of metastable PENNA dications. This in turn also suggests that strong field double ionization produced dominantly singlet open-shell dications. Closed-shell dications are unlikely to play a role due to their high excitation energies and barrierless reaction pathways, which should lead to the anisotropic angular distribution of the fragments.

Achieving 3D momentum-imaging of electrons at 10 kHz and beyond

Finally, we demonstrate another major improvement of the camera-based momentum-imaging system. For a typical coincidence measurement, because of the low count rate required for achieving true coincidence, it is preferred to have the whole system running at a repetition rate as high as possible. The limiting factor is usually the laser system. While one kHz laser is very popular and suitable for the camera-based 3D momentum-imaging setup, higher repetition lasers running at 10 kHz or 100 kHz do exist and are being used in many strong field experiments. By exploiting a simple fact of all coincidence measurements, we can improve the repetition rate of the current imaging system by five to ten folds without upgrading the camera. The low count rate of a coincidence experiment means that not every camera frame has event-hits. For example, roughly 80% of the camera frames will be without event-hit if the camera frame rate is the same as the laser repetition rate and the count rate is kept below 0.2 events/laser shot. This suggests that the camera frame rate is not fully utilized in this way. A different way of running experiments is to expose a camera frame for more than one laser shot. As long as the average hit in the camera is close to one per camera frame, the camera event and digitizer event can be correlated to provide the three coordinates for 3D momentum imaging. Even if there are a few events in one camera frame, the brightness-intensity correlation will be able to correlate the times with the positions of the events. With this method, the camera frame rate can now be fully utilized while the system repetition rate is increased five to ten times beyond the highest camera frame rate. We demonstrated this using a 10 kHz laser located in the

Kapteyn/Murnane group at the University of Colorado Boulder. The camera was running at 2 kFrames/s and the laser at 10 kHz. A standard VMI system with a three-lens spectrometer was used to detect the photoelectrons arising from the strong field ionization of krypton. Because only electrons were of interest, no electrode-pulsing was employed. Figure 7 shows the 3D momentum distributions of the electron Newton cloud. The achieved spatial and temporal resolution was good while it took only 5 minutes to accumulate these events.

CONCLUSION

We demonstrate a new method to convert a standard VMI apparatus to a coincidence 3D momentum-imaging setup without modifying parts inside the vacuum chamber or the imaging detector. It should be noted that this setup is automatically capable of slicing the electron Newton sphere due to its excellent temporal resolution. The additional cost for adding a second camera is minimum. The current setup requires a high repetition laser in order to expedite the data acquisition. Further improvement of the multi-hit capability might enable this to be used with lower repetition lasers. Furthermore, we have shown that a high system repetition rate beyond the camera frame rate can be achieved.

With this new imaging setup, by measuring the KER of dissociative double ionization and comparing it with density functional calculations, we show that the main products of the strong field double ionization of PENNA are singlet diradicals, which dissociate into $N(CH_3)_2CH_2^+$ and C_6H_5–CH_2^+. The isotropic distributions of fragment ions suggest a long lifetime of the parent dications, which poses a challenge for future experiments that aim for the molecular/recoil frame ionization rate.

[1]C. J. Danby and J. H. D. Eland, Int. J. Mass Spectrom. Ion Phys. **8**, 153 (1972).

[2]I. Powis, P. I. Mansell, and C. J. Danby, Int. J. Mass Spectrom. Ion Phys. **32**, 15 (1979).

[3]T. Baer, Int. J. Mass Spectrom. **200**, 443 (2000).

[4]B. Sztáray and T. Baer, Rev. Sci. Instrum. **74**, 3763 (2003).

[5]A. V. Golovin, F. Heiser, C. J. K. Quayle, P. Morin, M. Simon, O. Gessner, P. M. Guyon, and U. Becker, Phys. Rev. Lett. **79**, 4554 (1997).

[6]J. A. Davies, J. E. LeClaire, R. E. Continetti, and C. C. Hayden, J. Chem. Phys. **111**, 1 (1999).

[7]D. Rolles, Z. D. Pešić, M. Perri, R. C. Bilodeau, G. D. Ackerman, B. S. Rude, A. L. D. Kilcoyne, J. D. Bozek, and N. Berrah, Nucl. Instrum. Methods Phys. Res., Sect. B **261**, 170 (2007).

[8]T. Weber, O. Jagutzki, M. Hattass, A. Staudte, A. Nauert, L. Schmidt *et al.*, J. Phys. B: At. Mol. Opt. Phys. **34**, 3669 (2001).

[9]M. Lebech, J. C. Houver, and D. Dowek, Rev. Sci. Instrum. **73**, 1866 (2002).

[10]T. Osipov, C. L. Cocke, M. H. Prior, A. Landers, T. Weber, O. Jagutzki, L. Schmidt, H. Schmidt-Böcking, and R. Dörner, Phys. Rev. Lett. **90**, 233002 (2003).

[11]A. M. Rijs, M. H. M. Janssen, E. t. H. Chrysostom, and C. C. Hayden, Phys. Rev. Lett. **92**, 123002 (2004).

[12]A. Vredenborg, W. G. Roeterdink, and M. H. M. Janssen, Rev. Sci. Instrum. **79**, 063108 (2008).

[13]A. T. J. B. Eppink and D. H. Parker, Rev. Sci. Instrum. **68**, 3477 (1997).

[14]D. Townsend, M. P. Minitti, and A. G. Suits, Rev. Sci. Instrum. **74**, 2530 (2003).

[15]M. Ryazanov and H. Reisler, J. Chem. Phys. **138**, 144201 (2013).

[16]S. K. Lee, F. Cudry, Y. F. Lin, S. Lingenfelter, A. H. Winney, L. Fan, and W. Li, Rev. Sci. Instrum. **85**, 123303 (2014).

[17]S. K. Lee, Y. F. Lin, S. Lingenfelter, L. Fan, A. H. Winney, and W. Li, J. Chem. Phys. **141**, 221101 (2014).

[18]A. H. Winney, Y. F. Lin, S. K. Lee, P. Adhikari, and W. Li, Phys. Rev. A **93**, 031402 (2016).

[19]R. Weinkauf, L. Lehr, and A. Metsala, J. Phys. Chem. A **107**, 2787 (2003).

[20]S. Lünnemann, A. I. Kuleff, and L. S. Cederbaum, Chem. Phys. Lett. **450**, 232 (2008).

[21]S. Lünnemann, A. I. Kuleff, and L. S. Cederbaum, J. Chem. Phys. **129**, 104305 (2008).

[22]J. C. Bush, M. P. Minitti, and P. M. Weber, J. Phys. Chem. A **114**, 11078 (2010).

[23]A. J. Jenkins, M. Vacher, M. J. Bearpark, and M. A. Robb, J. Chem. Phys. **144**, 104110 (2016).

[24]B. Mignolet, R. D. Levine, and F. Remacle, J. Phys. B: At., Mol. Opt. Phys. **47**, 124011 (2014).

[25]W. Cheng, N. Kuthirummal, J. L. Gosselin, T. I. Sølling, R. Weinkauf, and P. M. Weber, J. Phys. Chem. A **109**, 1920 (2005).

[26]L. Lehr, T. Horneff, R. Weinkauf, and E. W. Schlag, J. Phys. Chem. A **109**, 8074 (2005).

[27]M. J. Frisch *et al.*, ɢᴀᴜssɪᴀɴ, Revision GDV. IΦ9, Gaussian, Inc., Wallingford, CT, 2016.

[28]J. D. Chai and M. Head-Gordon, Phys. Chem. Chem. Phys. **10**, 6615 (2008).

[29]M. M. Francl, W. J. Pietro, W. J. Hehre, J. S. Binkley, M. S. Gordon, D. J. Defrees, and J. A. Pople, J. Chem. Phys. **77**, 3654 (1982).

[30]P. C. Hariharan and J. A. Pople, Theor. Chim. Acta **28**, 213 (1973).

[31]R. Krishnan, J. S. Binkley, R. Seeger, and J. A. Pople, J. Chem. Phys. **72**, 650 (1980).

[32]R. Dennington, T. Keith, and J. Millam, *GaussView 5.0* (Semichem Inc., Shawnee Mission, KS, 2009).

[33]H. P. Hratchian and H. B. Schlegel, J. Phys. Chem. A **106**, 165 (2002).

[34]B. Mignolet, R. D. Levine, and F. Remacle, Phys. Rev. A **89**, 021403 (2014).

[35]C. S. Lehmann, N. B. Ram, and M. H. M. Janssen, Rev. Sci. Instrum. **83**, 093103 (2012).

[36]S. Sun, B. Mignolet, L. Fan, W. Li, R. D. Levine, and F. Remacle, J. Phys. Chem. A **121**, 1442 (2017).

[37]Y. F. Lin, S. K. Lee, P. Adhikari, T. Herath, S. Lingenfelter, A. H. Winney, and W. Li, Rev. Sci. Instrum. **86**, 096110 (2015).